PCCP

PAPER

View Article Online
View Journal | View Issue

Cite this: *Phys. Chem. Chem. Phys.*, 2025, **27**, 16507

Vibrational signatures of carboxylic acid microhydration for the HyDRA project†

Noah O. Evers, Sophie M. Schweer and Martin A. Suhm *

Received 24th May 2025,
Accepted 12th July 2025

DOI: 10.1039/d5cp01964h

rsc.li/pccp

HyDRA aims at the systematic experimental characterisation of water vibrations in different microsolvation situations for the purpose of quantum chemistry benchmarking, where quantum chemistry involves suitable combinations of electronic structure and nuclear dynamics treatments. The current HyDRA database largely lacks acid microsolvation data. This is cured by the present contribution, which characterises neutral microhydrates of formic and acetic acid by supersonic jet FTIR and Raman spectroscopy. The centroid of the bound water OH stretching fundamental in the monohydrate of formic acid is located at 3535(4) cm^{-1}. Literature monohydrate spectra of benzoic acid are confirmed. A surprisingly abundant metastable monohydrate of the acetic acid dimer is identified. The empirical relationship between harmonic B3LYP carboxylic acid complexation shifts of water and the experimental OH stretching shifts is remarkably robust.

1. Introduction

The stepwise hydration of acids is one of the cornerstones in the understanding of acid–base chemistry and has consequently attracted much attention.[1,2] It is fair to say that rotational and thus structural spectroscopy has provided the most reliable input in this field,[3–6] whereas vibrational spectroscopy, notably the hydride stretching signature of acidic dissociation, has been plagued by limitations of different kinds (see, *e.g.* ref. 7 and references cited therein). This also has to do with the fact that a hydride stretching quantum of excitation often provides enough energy for proton transfer to and from the solvent. The resulting structural and electronic rearrangement is typically accompanied by rapid vibrational energy flow and the associated lifetime broadening usually disables high resolution spectroscopy. However, such dynamical processes among strongly coupled vibrational modes are obviously of interest and deserve closer investigation. It also appears that inorganic acid hydrates[5,6,8] have received more attention than organic acid hydrates.[3,4,9–11] The present contribution tries to alleviate these imbalances by presenting vibrational spectra of microhydrates of elementary organic acids, namely formic and acetic acid. By removing any direct environment[12] and most thermal excitation,[13] through supersonic jet preparation, our experimental results are particularly amenable to theoretical modelling. Beyond the specific interest in these simple organic acid hydrates, there is indeed a more general interest in extending the vibrational spectroscopy database of organic molecule mono- and dihydrates, for the training of theoretical models which reliably predict the water vibrational dynamics in such organic solute environments. After a first blind challenge for theory in this field (called HyDRA[14] for hydrate donor red shift anticipation) we are currently widening the training data base in preparation of future rounds of HyDRA blind challenges. These will provide objective metrics on how successful electronic structure theory combined with different nuclear dynamics treatments is in predicting the vibrational dynamics of solvating water.

In contrast to their complexes with methanol,[15,16] the complexes of the simplest carboxylic acids with water can be considered to be structurally well characterised.[3,4] They are known to simultaneously engage the first water as a hydrogen bond donor (towards the carbonyl group) and as a hydrogen bond acceptor (towards the acidic OH), see Fig. 1 (centre).

The somewhat strained cyclic arrangement in the 1 : 1 complexes (hydrogen bond angles as small as 120° (ref. 3)) allows for the two hydrogen-bonded protons to simultaneously exchange their binding partners, resulting in an equivalent structure where the carbonyl and acidic oxygens are swapped. Non-cyclic 1 : 1 isomers, *e.g.* from coordination of the other lone electron pair of the carbonyl group,[17] are high in energy. A second water (1 : 2) or a second acid unit (2 : 1) potentially lead to larger structural variety. Reduction of ring strain keeps the abundance of 1 : 1 complexes in competition with dihydrates (1 : 2) intrinsically low. The strong homodimerisation tendency of carboxylic acids to relatively hydrophobic, nonpolar, cyclic units[18] makes it kinetically difficult to insert a water

Institute of Physical Chemistry, University of Goettingen, Tammannstr. 6, 37077 Goettingen, Germany. E-mail: noah-oriol.evers@uni-goettingen.de, sschwee@gwdg.de, msuhm@uni-goettingen.de

† Electronic supplementary information (ESI) available: Experimental details and auxiliary data for the Results and discussion section. See DOI: https://doi.org/10.1039/d5cp01964h

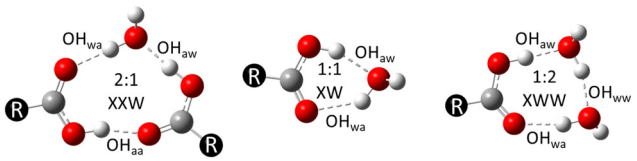

Fig. 1 Most stable mixed dimer (XW) and trimer (XXW, XWW) hydrogen bond topologies for formic (X = F, R = H), acetic (X = A, R = CH_3) and benzoic (X = B, R = C_6H_5) acid in combination with water (W). They are identified by their water-(w) or acid-based (a) OH donor stretching fundamentals, which are influenced by hydrogen bonding towards an acid (a) or water (w) neighbour acceptor, *e.g.* OH_{wa} for an OH group of W (w) coordinating the acid (a) in FW or AW.

molecule and increases competition by metastable 2 : 1 hydrates.[19,20] Indeed, the 1 : 1 complex is by far the mixed complex with the lowest average hydrogen bond energy.[21] In such a situation, it would be advantageous to use a size- and isomer-selective vibrational technique, often detected by cluster ionisation.[22] Applicable techniques which typically couple a UV and an IR photon usually profit from an aromatic chromophore. Even for benzoic acid, the accessibility of UV/IR double resonance techniques is limited to the trimer built from two acid and one water unit due to unfavourable processes in the electronically excited state.[11,20] If isomer selectivity is sacrificed, one can access size-selected infrared spectra with a VUV/IR technique, and this was previously explored for the 1 : 1 complex of benzoic acid with water.[11] In the present work, we use direct IR absorption and spontaneous Raman spectroscopy,[16] where size information can still be obtained in favourable cases by the variation of expansion conditions and where conformers can often be disentangled with the help of spectral predictions for the high frequency OH stretching fundamentals.

Such spectral predictions can be carried out at different levels of sophistication. Scaled harmonic DFT predictions provide a useful entry point,[16,23] in particular when comparing homologous systems. Unscaled harmonic frequencies are also available at CCSD(T) level for the simplest systems investigated in this work.[24,25] As an example, they suggest that the wavenumber splitting between the water and formic acid OH stretching vibrations in the 1 : 1 complex is significantly overestimated at MP2[12] and B3LYP level,[1,26] but the coupled cluster results themselves are strongly basis set dependent. Second order vibrational perturbation theory (VPT2) can improve the agreement,[11] but some of the error cancellation of harmonic DFT may get lost.[23,27] Occasionally, one has to treat close anharmonic resonances separately and solve them as an eigenvalue problem.[28] This is particularly true for higher order resonances, as they were recently found in monohydrates of carbonyl compounds.[29] The zero order states entering such a variational treatment typically already contain perturbational anharmonicity from other vibrational degrees of freedom. In this sense, the resonance parameters derived from experimental spectra are effective constants. Our work will highlight experimental evidence for such resonances in acid microhydrates, both within the solvating water unit and across the hydrogen bond.

To the best of our knowledge, the vibrational dynamics of microhydrated formic and acetic acid has not been investigated before in cold supersonic jet expansions. It has been addressed by matrix isolation spectroscopy[12,17,27,30] which shares the low temperature with supersonic jets, but includes spectral matrix shifts which are somewhat difficult to predict. Therefore, we will compare our gas phase work with the findings in the matrix. In this comparison, one has to distinguish two challenges for OH stretching vibrations. For the more weakly coupled vibration centred at the water, the challenge is to quantitatively remove environmental shifts for best use in benchmark calculations in the spirit of HyDRA.[14] For the more strongly coupled OH vibration centred at the carboxylic acid, the challenge is to observe it at all in the jet expansion, given that it is still elusive for the methanol complex,[16] but was reported for the hydrate complexes in some matrix studies.[12,17]

2. Methods

The FTIR and Raman supersonic jet spectrometers have been described elsewhere in the context of acid–alcohol clusters,[23] including the control of relative concentrations.[16] They differ in some essential technical details. Briefly, for the pulsed nozzle operation of the FTIR spectrometer, the hydrogen bond components were separately picked up by bubbling helium through the liquids kept below laboratory temperature and the two undersaturated gas mixtures were mixed with adjustable mixing ratios into a reservoir. From there, the supersonic expansion pulses through a long slit nozzle into vacuum were initiated. For the continuously operating Raman spectrometer, undersaturated helium gas mixtures were prepared analogously. Their mixing ratio was controlled by flow meters before expanding through a short slit nozzle into vacuum. Benzoic acid had to be kept above laboratory temperature (close to its melting point) for a sufficient vapour pressure and was picked up by a helium–water gas mixture, which had to be heated as well. The nozzle temperature was chosen slightly higher to prevent condensation. The FTIR beam probes a wide cross section of the expansion and thus averages over small and large nozzle distances, whereas the Raman excitation laser is focussed on a narrowly defined nozzle distance. In the FTIR spectrometer, the tiny (few ppm) attenuation of the IR beam is measured relative to a pre-pulse reference, whereas in the Raman spectrometer, feeble Stokes scattering is collected perpendicular to both the laser and the expansion direction and dispersed in a monochromator. For details, also concerning estimated compositions of the gas mixtures despite pronounced homodimerisation of the carboxylic acids and spectral subtraction procedures to minimise single component spectral contributions, see ref. 16. Suppliers and purities of the employed chemicals are given in the ESI† (Table S1).

Spectral intensities are less reliable than band positions, not only due to uncertainties in the composition and spectral overlap, but also due to non-uniform vibrational temperatures, noise level and technical issues such as averaging over wide expansion regions (FTIR) as well as frequency- and polarisation-dependent collection efficiencies (Raman). Nevertheless, qualitative comparisons in particular for nearby spectral features are

made and intensity centroids are also important for the approximate deperturbation of bright state/dark state resonances. Where needed, such intensity ratios and centroids were obtained by a Monte Carlo integration technique.[31]

Supporting calculations for the monomers (X = F, A, B) as well as their 1:1, 1:2 and 2:1 acid–water complexes (XW, XWW, XXW, Fig. 1) were carried out in the harmonic approximation using the B3LYP-D3(BJ) functional[32,33] in combination with the def2-QZVP basis set[34] using the ORCA 5.0.4 program suite (for keywords, see ESI,† Table S5).[35] The resulting electronic energy differences were corrected by unscaled harmonic vibrational zero-point energy contributions. This DFT level has proven to capture most of the relevant interaction contributions for hydrogen-bonded carboxylic acid complexes.[16,23] For the guidance of experimental assignments, the underlying harmonic wavenumbers (see ESI,† Table S6) were uniformly scaled by a factor of 0.98, which compensates for some density functional and harmonicity approximations.[23] Harmonically computed B3LYP intensities also help in guiding assignments, although one should not expect an accuracy better than a factor of two for intensity ratios due to numerous approximations in the theory-experiment comparison[36,37] (see ESI,† Table S6).

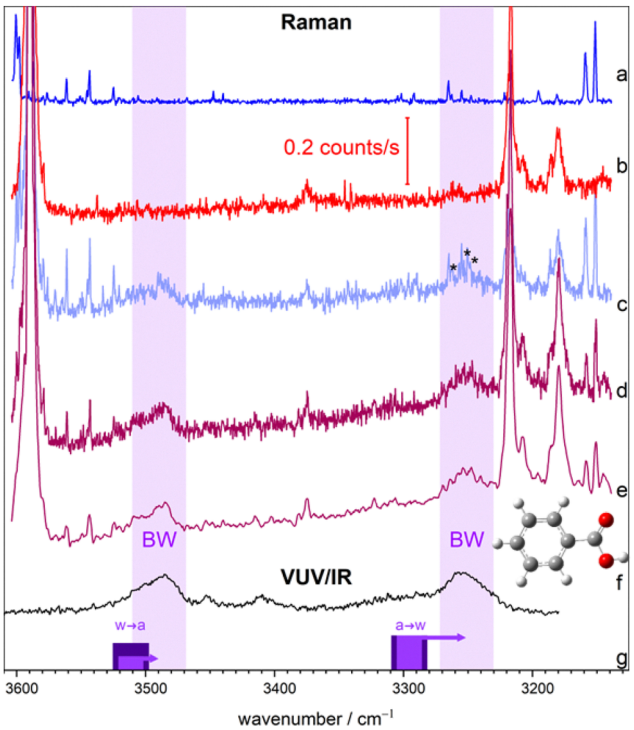

Fig. 2 Comparison of OH stretching signals in helium-seeded Raman jet expansions (uniform nozzle temperature 120–125 °C) of water (a) and benzoic acid (b) with mixtures of different relative concentrations (c) and (d). The mixtures aim at a constant product of the acid and water concentrations, such that 1:1 complexes should not change much in intensity. Trace (e) is a smoothened variant of (d), for best comparison to the size-selected VUV/IR spectrum[11] (f) for the 1:1 complex. Trace (g) shows relative harmonic Raman (light violet) and IR (dark violet) intensity at the scaled (0.98×) harmonic wavenumber positions for the water (w → a) and acid (a → w) vibration encoded as bar height. Arrows indicate the required shift to reproduce the experiment and coloured vertical ribbons qualitatively mark the core water- and acid-centred signal ranges. Sharp signals marked with ★ in this and other figures are due to fluorescent I_2 vapour impurities. See text for details.

3. Results and discussion

3.1. Validation with benzoic acid (B) monohydration

Because the vibrational spectroscopy of carboxylic acid monohydrates in supersonic jets is challenging, we start with a validation of our experimental approach for the case of benzoic acid. For that aromatic acid, spectra of the 1:1 complex with water[9] based on a powerful size-selective VUV/IR approach recently became available in the literature.[11] This spectrum is reproduced as trace f in Fig. 2. It consists of two clusters of broad IR signals below and above 3350 cm^{-1}. These correspond reasonably well to our scaled harmonic theoretical predictions (dark-violet bars in trace g, generic wavenumber scaling factor 0.98). Note that (uncoupled) diagonal anharmonicity alone would suggest a smaller scaling factor,[23] but DFT (in this case B3LYP-D3) deficiencies like delocalisation error in cooperative hydrogen bonds and off-diagonal anharmonicity (coupling to other vibrational states) do not support a clear decision between 0.98, 0.97 or 0.96, let alone a third decimal place for a generic DFT scaling factor on acid hydrates. The relative height of the dark-violet bars corresponds to the harmonically predicted relative IR intensities and is also seen to match the IR experiment in trace f reasonably well. Harmonic Raman intensities (in light violet) differ in predicting a lower relative scattering cross section for the higher-wavenumber (w → a) band.

Traces a–e in Fig. 2 illustrate the experimental Raman counterpart to this harmonic prediction. Trace a shows the rovibrational water monomer transitions[38] in a co-expansion of helium with water, trace b the corresponding spectrum of benzoic acid monomer (at the high-wavenumber end) and its dimer (at the low-wavenumber end with a small additional band in the centre). Traces c and d involve much more water than acid, but the product of the two concentrations is similar in the water-rich trace c and the acid-rich trace d, such that 1:1 complexes should form in similar amounts. This is true for two broad contributions highlighted with violet vertical ribbons, closely corresponding to the features in the size-selected VUV/IR spectrum. For the lower-wavenumber band, trace impurity iodine fluorescence peaks (★) render the comparison particularly difficult and superposition by mixed clusters of different stoichiometry cannot be ruled out, but overall the smoothened Raman spectrum in trace e attributed to the mixed complexes agrees remarkably well with the size-selected VUV/IR 1:1 complex spectrum in several details. The predicted reduced Raman intensity of the higher-wavenumber Raman band (trace g, harmonic B3LYP-D3(BJ)/def2-QZVP) relative to the VUV/IR spectrum is acceptably consistent with the experimental spectra (traces e and f), at least when all spectral features between 3380 and 3560 cm^{-1} are considered. It is difficult to say whether the harmonic intensity approximation, unassigned

anharmonic resonances or small contributions from larger clusters in the Raman spectrum should be invoked for remaining deviations.

For the HyDRA training database, an estimate of the intensity centroid in the higher wavenumber (water stretching) region has to be attempted. The centroid is the central wavenumber of an intensity pattern thought to arise from anharmonic couplings. It can be obtained by integrating over the normalised spectral intensity, weighted by its wavenumber. For our best estimate, we use the size-selective study.[11] The uncertainty is obtained from the integration uncertainty and the change in centroid when the two weak bands near 3400 and 3450 cm^{-1} are left out or when the Raman spectrum is integrated instead of the VUV/IR spectrum. A centroid of 3490 ± 10 cm^{-1} covers all three estimates and shall be used for the entry in the HyDRA training database. For the dominant transition alone, our best estimate based on the intensity centroids for the IR and Raman spectra and variation in the integration range is (3494 ± 2) cm^{-1} whereas the actual dominant peak wavenumber is about 3485 cm^{-1} (trace e and f [11]). This dominant transition due to the hydrogen-bonded water OH group accounts for 90 ± 10% of the intensity in the VUV/IR and Raman spectra above 3380 cm^{-1}. The centroid for the acid stretching fundamental is less certain due to the broad shoulder around 3300 cm^{-1} (in the VUV-IR and the Raman spectrum) which may or may not be part of the transition. We refrain from an estimate, because for the HyDRA challenge, only the w → a position is relevant. The light violet arrow in Fig. 2 pointing to 3252 cm^{-1} only gives a rough orientation for the experimental center of the transition, if the shoulder around 3300 cm^{-1} is not included.

There is no direct spectral evidence for 1 : 2 or 2 : 1 benzoic acid water complexes in the Raman jet spectra, but previous work using UV[20] or VUV[11] detection suggests that these complexes involve several populated conformations and anharmonic resonances over a wide spectral range. Even the conformationally selective spectrum of the 2 : 1 complex[20] shows significant complexity. Therefore, benzoic acid only serves as a guidance for the 1 : 1 hydrate complexes of simpler carboxylic acids, which will be discussed in the following.

3.2. Formic acid (F) microhydration

Formic acid is much more accessible to high level full-dimensional theoretical treatments than benzoic acid. The first cold gas phase vibrational spectra for its clusters with water are presented in Fig. 3. As usual in carboxylic acid–solvent complexes, the distinction between mixed dimeric and trimeric clusters of F and W based on intensity scaling with concentration is not simple, due to substantial cooperativity effects and the strong competition by acid homodimers. Nevertheless, Fig. 3 proposes an initial assigment based on IR and Raman spectra in the OH stretching range.

The assignment (in terms of coloured vertical ribbons) of FFW, FW and FWW (with increasing tentativeness in this sequence) is based on three Raman (upper, a–c) and three IR spectra (lower panel, e–g) with varying relative concentration.

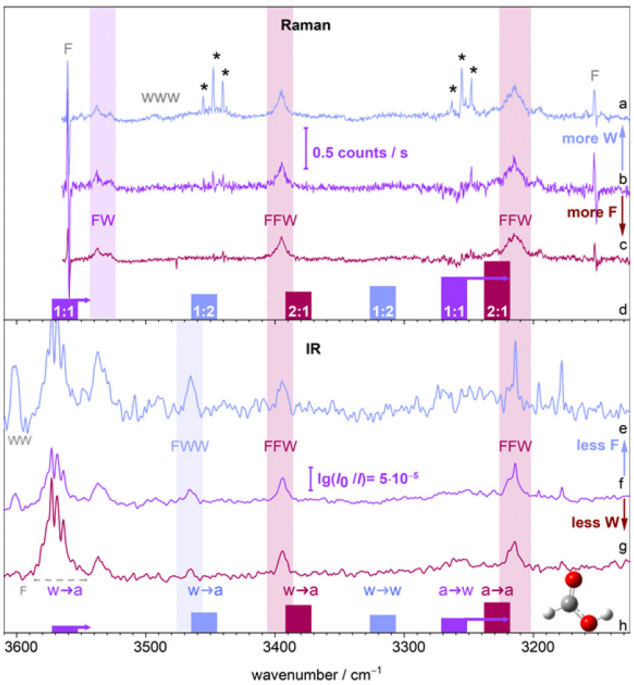

Fig. 3 Raman (a)–(c) and IR spectra (e)–(g) of formic acid–water expansions for different composition after subtraction of monomer contributions (for raw spectra see ESI,† Fig. S3) in comparison to 0.98× wavenumber-scaled harmonic B3LYP-D3(BJ)/def2-QZVP predictions (d for Raman, h for IR). Arrows transfer the theory error from benzoic acid (Fig. 2) to formic acid. All spectra are intensity-scaled to the 3396 cm^{-1} transition in the violet spectral traces assigned to FFW (see ESI,† Table S10 for scaling factors). The spectral trace colour reflects more water-rich (blue) and more acid-rich (purple) expansions, keeping the concentration of the other component approximately constant. F marks poorly compensated formic acid monomer, WW (WWW) the water dimer (trimer).[39] See text for explanations.

It is also supported by the pioneering microwave identification of these organic acid hydrates.[3] Water-rich spectra are shown in blue, acid-rich spectra in purple, roughly equimolar expansions in violet. Vertical arrows between spectra indicate which species concentration changes and are given the colour of the component made dominant. All spectra are scaled in their intensity to the transition at 3396 cm^{-1}, which most likely corresponds dominantly to FFW, the 2 : 1 complex. It has a counterpart at 3215 cm^{-1} (with a very weak satellite peak in the Raman at 3196 cm^{-1} which cannot be assigned to a specific cluster size and is not exclusively due to water monomer bend overtone transitions). The two bands match the uniformly scaled harmonic DFT predictions (purple bars in traces d and h) reasonably well, both in position and in relative intensity. The higher-frequency transition corresponds to water vibrating against an acid unit (w → a), whereas the lower-frequency transition corresponds to acid pairing (a → a). The a → w transition falls out of the displayed spectral range, but remains elusive (see ESI,† Fig. S1), as for the methanol complex of formic acid.[16] This is shown by C-deuteration, which removes overlapping CH stretching transitions.

A closely spaced pair of Raman signals near 3538 and 3528 cm^{-1} scales like FFW with increasing water concentration,

but less strongly than FFW with increasing acid concentration, although this trend is quite subtle. Such a scaling behaviour indicates that the underlying complex contains one water unit (as FFW does) and one acid unit (less than FFW). The IR counterpart is less conclusive due to overlap with an IR-active water homotrimer signal (at 3533 cm^{-1})[40] and a CO overtone of the acid (at 3538/3533 cm^{-1}).[41] The Raman doublet is thus tentatively assigned to a mixed dimer FW which is expected in that region based on the scaled harmonic approximation (violet bar in trace d) and the offset found for B. As only a single w → a band is harmonically predicted, we invoke an anharmonic resonance for the doublet appearance and any comparison with harmonic theory should be made based on the intensity centroid of the doublet near 3535 cm^{-1}, to which we assign an uncertainty of ±4 cm^{-1}. An alternative assignment to a tunneling splitting due to large amplitude free OH flipping across the molecular plane is unlikely by comparison to a colder expansion in neon carrier gas (ESI,† Fig. S9).

There is little evidence for a corresponding FW signal of the a → w vibration predicted between 3300 and 3200 cm^{-1}, which should be stronger in intensity than the w → a transition in both IR and Raman spectra (violet bars in traces d and h). This could be due to excessive resonance splitting, dissipative lifetime broadening, overlap with the strong a → a FFW signal or interference from I_2 impurity fluorescence (Raman, *). It is reminiscent of the formic acid methanol situation,[16] where the absence of the acid vibration in the 1 : 1 complex was even clearer. In contrast to the benzoic acid monohydrate, we thus refrain from an assignment of this FW a → w vibration in the jet spectra but the violet arrow in trace g indicates based on the benzoic acid analogy where to expect the center of the elusive transition. Evidence for the water-rich FWW trimer is also weak and restricted to the IR, with only one signal at 3466 cm^{-1} showing the expected relative intensity increase with less F content. This would be consistent with the scaled harmonic w → a prediction for FWW, but the absence of a Raman counterpart and the uniform lack of evidence for the corresponding w → w transition near 3300 cm^{-1} as well as an a → w transition renders such an assignment very speculative (see Table S12 in the ESI†). It is less relevant for the present work and will therefore not be followed up. The proposed FFW (3396 cm^{-1}) and FW (3535 cm^{-1} doublet) w → a assignments are more robust and their signals can also be differentiated by changing the nozzle temperature in the Raman experiment (Fig. 4). The 1 : 1 cluster signal loses in intensity relative to the 1 : 2 signal (which is kept constant by intensity scaling), if the nozzle temperature decreases. The latter supports the formation of larger clusters and formic acid dimers and therefore the assignments.

Further evidence for the mixed dimer and trimers comes from deuteration of the OH bond of both binding partners (Fig. 5). The resulting Raman OD stretching spectra (inverted for better distinction; purple with more, violet with less acid) can be roughly frequency-scaled to the OH stretching spectrum from Fig. 3 by a factor of 1.35 to demonstrate the signal correspondence. For this purpose, the spectra are intensity-scaled to the same FFW signal as before. Three things are notable: The splitting of the FW w → a signal is removed for OD, supporting a resonance interpretation in the OH stretching range. The intensity of the single FW peak in the OD stretching spectrum scales less strongly with acid concentration than FFW, supporting its FW assignment. Instead of the weak unassigned a → a FFW satellite at 3196 cm^{-1} a more symmetric doublet emerges upon deuteration, suggesting a new resonance situation in the OD stretching range.

One can speculate about possible resonance partners based on harmonic wavenumber predictions. For the 3538/3528 cm^{-1} OH doublet (w → a), an effective coupling matrix element can be estimated by assuming that the resonance partner has no intrinsic Raman intensity. With about 5 cm^{-1}, the coupling is weaker than in ketone hydrates,[29] where a robust resonance with a three-quantum state (b2lib) and a coupling matrix element of about 10 cm^{-1} was found in this spectral range. An analysis including the removal of the resonance upon deuteration is given in the ESI† (Section S2.5). We thus assume a b2lib resonance for the w → a vibration in FW, but for benchmarking purposes it is only important that there is a

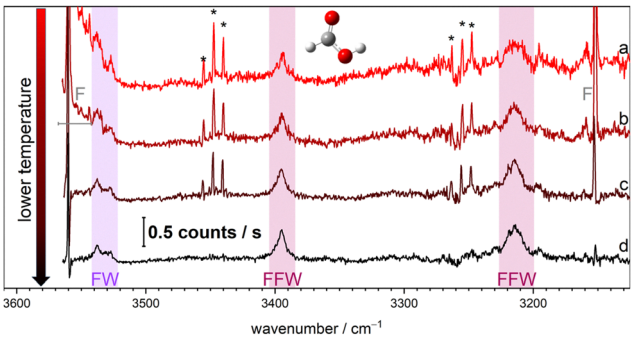

Fig. 4 Raman intensity trends (scaled to the FFW band at 3396 cm^{-1}) for signals due to FW (violet) and FFW (purple) complexes (after subtraction of room temperature nozzle one-component spectra of F to cancel FF homodimer contributions) as a function of decreasing nozzle temperature from top (≈350 K) to bottom (room temperature). See ESI,† Table S3 for details.

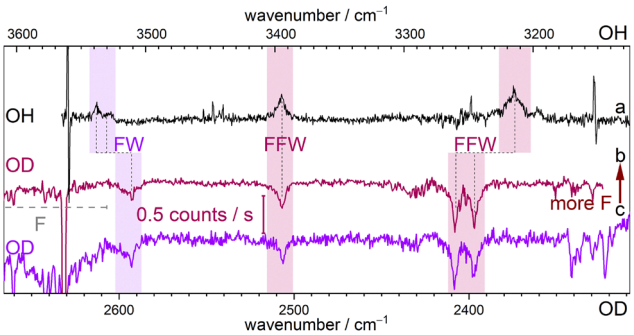

Fig. 5 Raman jet spectra before (trace a, same as trace b in Fig. 3) and after deuteration of F and W (trace b with more F and trace c with less F; inverted), intensity scaled to the FFW w → a transition. To qualitatively remove the isotope effect, the OD spectra were wavenumber-stretched by 1.35, so that the monomeric formic acid band positions match for both isotopes.

resonance with some dark combination state and that the stronger of the two signals only represents a fraction of about 0.60–0.75 of the OH stretching character. For the more asymmetric 3215/3196 cm^{-1} doublet near a → a of FFW, a remote resonance explanation is unlikely because the doublet is not repeated in the IR (Fig. 3). In contrast, upon deuteration, the intensity pattern suggests a strong resonance around 2400 cm^{-1}. Specifically, Fermi coupling between the acid-based OD-stretching vibration and the (heavy) water bending overtone might be postulated. The underlying coupling constant derived from spectral intensities (Section S3.4 in the ESI†) would be 6 cm^{-1}. Although it would formally be a resonance across molecules, the mixed character of the concerted OD stretching vibrations together with a strong coupling of the water bending overtone with the water OD stretch[38,39] support such an interpretation. Extension of the deuteration experiment to the IR and anharmonic calculations will be needed to clarify the situation. In any case, our spectra contain no evidence for isomeric complexes of formic acid hydrates.[1]

Finally, the present vacuum-isolated complex results may be compared to previous argon matrix isolation assignments[12,27] (Table 1). We neglect complexation of *cis* formic acid,[43] which is not significantly populated under the current conditions in the jet expansions.[44] An interesting matrix aspect is that the resonance assigned for the w → a band is removed, unless the second component is hidden under a water trimer signal. Such environment-dependent subtle resonances are not unprecedented, if matrix shifts of the interacting states exceed the coupling matrix element.[45,46] In this situation, it is particularly important to work with intensity centroids when comparing gas phase and matrix values. Doing that, we find an excellent agreement for the w → a band positions of FW between gas and matrix environments, independent on the isotope. Normally, one would expect significant spectral matrix downshifts for hydrogen-bonded systems (even more than for the monomers which are also listed in Table 1), so the close agreement is surprising and might even cast doubt on either the gas phase or matrix assignment. However, one should consider that FW is a quasiplanar complex, and the matrix could easily force the dangling water OH into the plane of the molecule. Exploratory harmonic frequency calculations (ESI,† Table S8) suggest that this planarisation raises the hydrogen-bonded OH wavenumber by tens of cm^{-1}, thus potentially counteracting any intrinsic matrix-induced downshift for hydrogen-bonded OH oscillators.[46] Perhaps the monohydrate of formic acid behaves like some other planar and quasiplanar cooperative systems with hydrogen bond strain ($(HF)_3$, $(CH_3\ OH)_3$), where argon matrix shifts are also anomalously small or even opposite in sign.[47,48] For FFW we are not aware of a matrix assignment with which we could compare. The FWW dihydrate matrix downshift, where the jet assignment is more tentative, would be more in line with expectations for typical matrix shifts for hydrogen-bonded systems. Turning to the jet-elusive a → w band of FW, the previous matrix work may provide further insights. If a similar compensation between matrix embedding (downshift) and matrix planarisation (upshift) as in the w → a case is postulated, FFW and FW overlap in this spectral range of the jet spectrum is conceivable. In one argon matrix study[12] the FW signal is assigned at 3212 cm^{-1}. This is confirmed in one other matrix study[43] but left open in another one.[27] If correct and associated with a small matrix shift, it would suggest that the FW a → w signal in the jet is hidden under FFW. Perhaps the weak 3196 cm^{-1} Raman signal is part of the FW signature, with more contributions hidden at higher wavenumbers. In summary, the only safe vibrational assignments of free formic acid hydrate complexes are the w → a transitions of FW and FFW as well as the a → a transition in FFW. This restricted vibrational evidence for formic acid hydrate complexes calls for an investigation of another homolog of formic acid, acetic acid.

Before moving to acetic acid, it is instructive to compare observed complexation shifts of water OH (OD) fundamentals in formic acid water complexes (in the jet, without matrix influence, relative to the symmetric stretch of the water monomer) with harmonic complexation shifts predicted by our exploratory DFT approach (without anharmonic effects). Naively, one might expect that the ratio is close to 1, because at least the diagonal anharmonic effects (along the OH or OD stretching coordinate) should largely cancel between the water monomer and the complex. If anything, the jet downshifts should be slightly larger because the OH/OD bonds are elongated and thus softened in the hydrogen bond, which is not fully captured in the harmonic approximation. Table 2 shows that the opposite is the case. The experimental anharmonic shifts only amount to slightly more than 2/3 of the harmonic predictions. Two effects may be held responsible: The delocalisation error of the hybrid functional overestimates the cooperativity of the hydrogen bond and there are substantial off-diagonal anharmonic effects which weaken the hydrogen bond through motion perpendicular to it. From the HyDRA perspective of predictability of the experimental shifts, it is rewarding that the ratio between the jet complexation shift and the harmonic DFT complexation shift is remarkably constant at 0.71 ± 0.03 when water is involved.

Table 1 Comparison of experimental jet and matrix band positions[12,42] for formic acid hydrates and their components. A superscript * marks band centroid positions, where intensity redistribution due to vibrational resonances is assumed. Values in parentheses mark very tentative assignments. Spectral Ar matrix shifts Δ in cm^{-1} are also listed, where available

Complex	Vib.	$\tilde{\nu}_{jet}/cm^{-1}$	$\tilde{\nu}_{Ar}{}^{12}/cm^{-1}$	Δ
FW	OH_{wa}	3535*	3537	+2
FW	OD_{wa}	2594	2593	−1
FW	OH_{aw}	—	3212	
FWW	OH_{wa}	(3466)	3441	(−15)
FFW	OH_{wa}	3396	—	
FFW	OD_{wa}	2507	—	
FFW	OH_{aa}	3215	—	
FFW	OD_{aa}	2401*	—	
F	OH	3570[41]	3550	−20
F	OD	2631	2618[42]	−13
W	OH (asym)	3756	3732	−24
W	OD (asym)	2788	2771	−17
W	OH (sym)	3657	3640	−17
W	OD (sym)	2671	2658	−13

Table 2 Comparison of jet-cooled water wavenumber downshifts $\Delta\tilde{\nu}_{jet}$ (in cm^{-1}) in the hydrate complexes of formic acid (F) relative to the symmetric stretch of monomeric water (W) with the corresponding harmonic DFT predictions $\Delta\omega_{th}$. The ratio $\Delta\tilde{\nu}_{jet}/\Delta\omega_{th}$ is remarkably constant and remarkably smaller than 1

Cluster	Vib.	$\Delta\tilde{\nu}_{jet}$	$\Delta\omega_{th}$	$\Delta\tilde{\nu}_{jet}/\Delta\omega_{th}$
FW	OH_{wa}	122	171	0.71
FW	OD_{wa}	77	111	0.69
FWW	OH_{wa}	(191)	281	(0.68)
FFW	OH_{wa}	261	355	0.74
FFW	OD_{wa}	164	237	0.69

3.3. Acetic acid (A) microhydration

The replacement of the CH bond in F by a bonded methyl group leads to acetic acid (A) with analogous mixed dimers and trimers involving water (AW, AWW, AAW). It also leads to an energy lowering for metastable species, which we mark with a star in Fig. 6. These were not relevant in the jet expansions of formic acid with water, but in particular the AAW* structure falls into an energy range where a sufficiently high barrier to isomerisation can hinder the relaxation to the global minimum structure. The relaxation barriers (‡) are also encoded in Fig. 6 as numbers next to the connecting arrows. As AAW* formation from the constituents AA (or even A + A) and W is essentially barrierless, it can get kinetically trapped if the AA formation precedes the AW formation. Note that AAW* depicted in Fig. 6 (previously considered for FFW,[3,22] AAW[19] and BBW[20]) is much more stable than the metastable AAW trimer proposed earlier.[17]

Indeed, Fig. 7, which is analogous to Fig. 4, contains more spectral signatures of mixed acid–water complexes. Instead of 3 regions with about 5 spectral bands for F + W, 6 regions with about 10 bands can be identified for A + W. The spectra involve varying nozzle temperatures and are intensity scaled to similar signal strength at 3374 cm^{-1}, near the FFW band to which formic acid spectra were scaled in Fig. 4. In analogy to F, this is believed to be the stretching fundamental of the hydrogen-bonded water OH bond in AAW (see below). The acetic acid OH

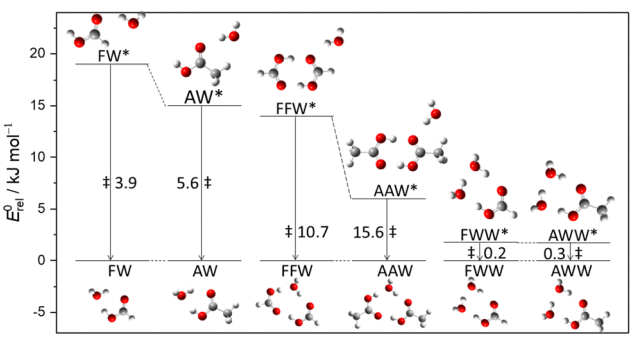

Fig. 6 Effect of the extra methyl group in acetic acid on the energy and stability of metastable (*) acid hydrate isomers. It consistently lowers their energy but tends to increase high interconversion barriers (‡, in kJ mol^{-1}) relative to the global minimum structures. The effect is most pronounced for AAW*, which may thus be expected to be stabilised in a jet expansion. See ESI,† Table S7, for energy values.

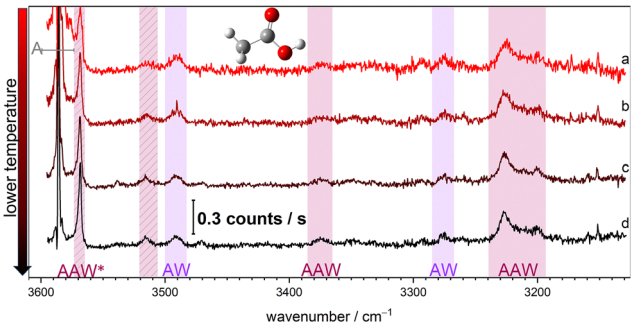

Fig. 7 Raman intensity trends (scaled to the AAW band at 3374 cm^{-1}) for signals due to AW (violet) and AAW (purple, shaded for metastable) complexes (after subtraction of room temperature nozzle one-component spectra of A to cancel AA homodimer contributions) as a function of decreasing nozzle temperature from top (≈350 K) to bottom (room temperature). See ESI,† Table S3, for details.

counterpart in AAW (OH_{aa}) is a pronounced doublet with a similar scaling behaviour and both bands are marked in purple (although it is not clear whether they have the same origin). Two weak bands marked in violet gain in relative strength when the nozzle temperature increases, indicating their mixed AW dimer origin. They are flanked by even weaker signals which are more difficult to assign (see Table S12 in the ESI†). The most prominent and highest wavenumber cluster band (hashed purple) shows a slight decrease in intensity with increasing nozzle temperature and has no counterpart for F. It must correspond to either a larger cluster or more likely a metastable trimer. This is also a possible interpretation of the second signal hashed in purple (near 3516 cm^{-1}), whereas the signal flanking the w → a AW dimer signal from the other side is due to a cluster with more than one water unit. We are unable to provide fully convincing explanations for these flanking signals and will leave their assignment open from now on. Because there is the remote possibility that they hide b2lib resonance partners of the w → a band of AW at 3491 cm^{-1}, we double its overall intensity centroid uncertainty (±8 cm^{-1}) relative to FW.

Clearly, the increased complexity observed in the hydrate spectra of A compared to those of F requires further experimental and theoretical (scaled harmonic B3LYP-D3(BJ)/def2-QZVP) evidence. This is summarised in Fig. 8, where different Raman spectra are intensity-scaled to the AAW transitions in trace b of the upper panel, in analogy to what was done in Fig. 3 for FFW. Differences in scaling behaviour for AW complexes when adding more A (trace c) or more W (trace a) are less pronounced, but still consistent with less A and equal W content in the mixed dimer. Very instructive is the ^{18}O isotope substitution for water (trace d), which unambiguously shows that the four strongest transitions above 3300 cm^{-1} have water stretching character, whereas the strong mixed cluster signal below 3300 cm^{-1} has acid OH character and does not shift upon water isotope substitution. This is consistent with the scaled harmonic predictions shown in trace e, where arrows on the AW transitions transfer the theory error from B (Fig. 2) to A. The ^{18}O isotope substitution is crucial for the assignment of

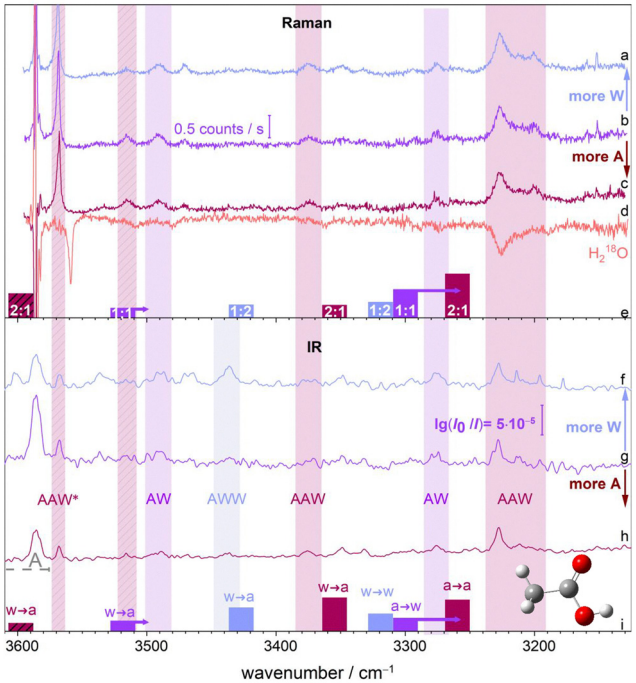

Fig. 8 Comparison of Raman (a)–(d) and IR (f)–(h) jet spectra from co-expansions of A and W with scaled harmonic theory (e) and (i) in analogy to Fig. 3, besides the metastable complexes. The spectra show evidence for mixed dimers and mixed trimers, the latter also as metastable intermediates with high relaxation barrier. Oxygen isotope substitution (d) allows to distinguish between water-based and acid-based vibrations. See text for further explanations and the ESI† (Section S3.3) for Raman spectral subtraction procedures.

AAW* (hashed purple), because a competing assignment to AW*[17] would be acid-centered and thus lack the isotope shift.

From left to right, we thus have one or perhaps two metastable AAW* trimer signals (hashed purple) and a first AW signal, all due to water-centred stretching vibrations. Further to the right, two AAW vibrations are found in close analogy to FFW (in both cases, harmonic theory underestimates their splitting). Between them, in contrast to the F case but in good agreement with the B case, there is now clear evidence for the acid OH vibration (a → w) in the mixed AW dimer. When increasing the water concentration (trace a), all marked signals behave similarly or even decrease in relative intensity (3516 cm^{-1}), therefore none of them is expected to contain two water units. In analogy to the case of F, the Raman spectra thus show little evidence for a water-rich trimer, but the IR spectra (lower panel) again provide speculative evidence for at least one AWW band, which exhibits the expected scaling with increasing W. Most other bands assigned in the Raman spectra are also present in the IR spectra and show a consistent scaling behaviour. However, the predicted intensity ratio for the two AAW transitions does not agree well with experiment. This may be related to a triplet-like band pattern observed in the IR at high acid concentration around 3350 cm^{-1} (but also discernible in some of the Raman spectra). One explanation for this and other small spectral features may be coupling to low frequency modes, in particular methyl torsion which is absent in F (ESI,† Table S9). In any case we refrain from using the AAW transition for benchmarking purposes.

Despite these intensity inconsistencies, one can still try to derive an approximate range of abundance ratios AAW*/AAW consistent with the various helium slit jet expansions. This must include uncertainties in calculated intensities, choice of vibrational bands, potential redistribution effects due to vibrational coupling, and variation with expansion conditions like nozzle temperature. Our best estimate for this ratio is 1–3, which is uncertain but still large considering an energy penalty of more than 5 kJ mol^{-1} for the AAW* isomer. This clearly points at kinetically controlled formation of AAW* from preformed AA dimers and W units. In any case, the newly assigned AAW* complex has significant model character for the competition between dissociation and tunneling processes in hydrated AA dimers.[18]

As for formic acid, theory agrees reasonably well with the experiment in predicting the HyDRA-relevant downshifts of the hydrogen-bonded water stretching vibration from the symmetric stretch of water monomer in complexes with acetic acid (A), when the harmonic prediction is scaled by 0.72 ± 0.06 (Table 3). The scaling factor for benzoic acid (B) also falls into this range in a case of remarkable error cancellation between the DFT and harmonic approximations. If one were to include anharmonic effects, deficiencies of the underlying DFT functional would likely become visible and the jet/th(eory) ratio would probably not become more uniform, let alone approach unity. Nevertheless, such fortuitous cancellations can be useful for interpolation between related systems.

Comparison to the Ar matrix results[17] for the acetic acid hydrates is made in Table 4. In contrast to FW, where the matrix shift for the hydrogen-bonded water stretching vibration was negligible (Table 1), there is now a sizeable upshift by the Ar matrix for AW instead of the typical downshift for hydrogen-bonded systems. This is highly unusual and not explainable with uncertainties in the jet band positions or planarisation effects due to the matrix. Interestingly, a similar band position was observed in N_2 matrices.[25] A comparison to the recently investigated glycolic acid monohydrate[49] where a structure analogous to that of acetic acid monohydrate was predicted to be the most stable and dominant, can provide further hints.

Table 3 Comparison of jet-cooled water wavenumber downshifts $\Delta\tilde{\nu}_{jet}$ (in cm^{-1}) in the identified hydrate complexes of acetic acid (A) and benzoic acid (B) relative to the symmetric stretch of monomeric water with the corresponding harmonic DFT predictions $\Delta\omega_{th}$. The ratio $\Delta\tilde{\nu}_{jet}/\Delta\omega_{th}$ is again remarkably smaller than 1 and quite uniform. The AW ratio might be somewhat lower if there is an anharmonic resonance shifting the state to lower wavenumber (see text)

Cluster	Vib.	$\Delta\tilde{\nu}_{jet}$	$\Delta\omega_{th}$	$\Delta\tilde{\nu}_{jet}/\Delta\omega_{th}$
AW	OH_{wa}	166	216	0.77
AWW	OH_{wa}	(221)	309	(0.72)
AAW	OH_{wa}	283	383	0.74
AAW*	OH_{wa}	89	135	0.66
BW	OH_{wa}	167	223	0.75

Table 4 Comparison of experimental jet and matrix band positions for acetic acid (A) and its water complexes (W). Spectral Ar matrix shifts Δ in cm^{-1} are also listed, where available

Complex	Vib.	$\tilde{\nu}_{jet}/cm^{-1}$	$\tilde{\nu}_{Ar}{}^{17}/cm^{-1}$	Δ
AW	OH_{wa}	3491	3534	+43
AW	OH_{aw}	3277	3208	−69
AW*	OH_a	—	3582	
AW*	OH_{wa}	—	3499	
AWW	OH_{wa}	3436	—	
AAW	OH_{wa}	3374	—	
AAW	OH_{aa}	3217	—	
AAW*	OH_{wa}	3568	—	
A	OH	3586	3566[52]	−20

The additional alcoholic OH oscillator is only weakly coupled to the acidic OH and should therefore not introduce complications.[50] Harmonic theory would predict water bound to glycolic acid to absorb at considerably higher wavenumber than for the acetic acid case (about 60 cm^{-1}, see ESI,† Table S6), whereas the matrix experiments suggest a difference of less than 10 cm^{-1}. Hence, the monohydrate of acetic acid shows matrix anomalies in comparison to formic and glycolic acid.

For the OH_{aw} transition of AW, which was elusive in the jet spectrum of FW, a more conventional wavenumber downshift is observed in the Ar matrix. In an N_2 matrix, three transitions separated by more than 100 cm^{-1} were assigned to this transition, all of them again downshifted from the jet assignment.[25] Part of this opposing matrix behaviour for the two OH oscillators may stem from an increased harmonic coupling of the two H oscillators in the matrix, which would raise the upper wavenumber and at the same time lower the lower one. In any case, assuming that the jet and matrix assignments are correct, the matrix shifts for acid monohydrates turn out to be quite unpredictable or at least unsystematic. Possible control experiments include matrix shifts for formic and acetic acid with dimethylether[51] or other exclusive hydrogen bond acceptors.

4. Conclusions

Unambiguous spectral assignments of isolated carboxylic acid water complexes are challenging, but rewarding due to the enormous complexity of the condensed phase situation.[53] For the purpose of the HyDRA benchmark database and future blind challenges, we have derived conservative experimental values for the hydrogen-bonded OH-stretching mode of water in 1 : 1 complexes. For benzoic acid, we confirm a value of 3490 ± 10 cm^{-1}, for formic acid we find 3535 ± 4 cm^{-1} after deperturbation of a local resonance (3538 ± 2 cm^{-1} for the main signal which carries 60–75% OH-stretching character; 3528 ± 2 cm^{-1} for the secondary signal), and for acetic acid, we find 3491 ± 8 cm^{-1}. These acid-coordinating water vibrations are summarised in Fig. 9 together with those of water molecules coordinating acid dimers (XX). For the latter, only FFW is unambiguous enough for benchmarking purposes and we assign an experimental wavenumber of 3396 ± 2 cm^{-1} together with an OH stretching fractional character of at least 90%. AAW* is also clearly assigned, but due to its metastability it does not qualify for the HyDRA database.

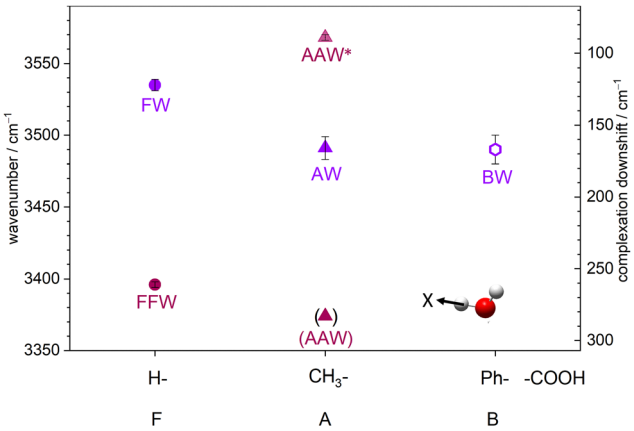

Fig. 9 Assigned hydrogen bonded water (W) OH stretching fundamentals in XW and XXW complexes (X = F, A, B) from this work (for BW in agreement with a previous VUV/IR study [11]). Where the symbol size exceeds the uncertainty, no error bar is shown. The AAW position (in parentheses) is very uncertain due to satellite bands.

The acid vibration in the 1 : 1 complexes is more difficult to locate. For benzoic and acetic acid, it gives rise to broad signals in the range of 3250–3300 cm^{-1}, for formic acid it remains elusive, either due to extensive resonances or due to spectral overlap. The former explanation was considered to be more likely in the related case of the 1 : 1 complex of formic acid with methanol.[16] Although acidic OH bond dissociation requires many solvating waters,[54,55] already the first water molecule may induce dissipative dynamics upon acid OH excitation. By embedding the 1 : 1 complexes in Ar matrices, the detection sensitivity is increased, but the resulting matrix shifts on the OH stretching vibration appear to behave quite irregularly, where they are experimentally available.

Because carboxylic acid complexes are emerging as suitable test objects for relatively large discrepancies observed between high-level electron correlation methods,[56] the present work may even become useful beyond the prediction of anharmonic vibrational energy levels. Nuclear quantum effects stand between electronic structure theory and experiment in hydrogen bonding. The better one can predict these anharmonic motions, the more helpful experiment can be in adjudicating between different quantum chemical approximations.

In conclusion, the present contribution provides firm experimental reference points for OH stretching vibrations in small microhydrated carboxylic acids. By avoiding thermal, matrix, and bulk solvation perturbations and by focussing on relatively isolated high frequency modes, these reference points invite high level quantum chemical calculations with appropriate low- or high-dimensional nuclear quantum treatments to close the gap between theory and experiment.

Conflicts of interest

There are no conflicts to declare.

Data availabilty

The data supporting this article have been included as part of the ESI.† In addition, the original Raman and infrared spectra and the.xyz files from the harmonic calculations are made available at the GRO.data repository at **https://doi.org/10.25625/5TXBGE**.

Acknowledgements

We thank M. Bödecker, M. Niessner, and E. Sennert for helpful discussions. We are grateful to Y. P. Lee for providing a VUV/IR spectrum for benzoic acid monohydrate.[11] Our study is dedicated to the late T. Ebata, an encouraging pioneer in the combined use of IR and Raman jet spectroscopy for hydrogen-bonded complexes. This work was funded by the Deutsche Forschungsgemeinschaft (DFG, German Research Foundation) - 465181753 (SU 121/8-1) and its benchmarking aspects were promoted by the research training group GRK2455 (project 389479699).

References

1 S. Aloisio, P. E. Hintze and V. Vaida, *J. Phys. Chem. A*, 2002, **106**, 363–370.
2 A. Bende, G. Perretta, P. Sementa and T. M. Di Palma, *Chem. Phys. Chem.*, 2015, **16**, 3021–3029.
3 D. Priem, T.-K. Ha and A. Bauder, *J. Chem. Phys.*, 2000, **113**, 169–175.
4 B. Ouyang and B. J. Howard, *Phys. Chem. Chem. Phys.*, 2009, **11**, 366–373.
5 K. R. Leopold, *Annu. Rev. Phys. Chem.*, 2011, **62**, 327–349.
6 F. Xie, D. S. Tikhonov and M. Schnell, *Science*, 2024, **384**, 1435–1440.
7 M. Letzner, S. Gruen, D. Habig, K. Hanke, T. Endres, P. Nieto, G. Schwaab,. Walewski, M. Wollenhaupt, H. Forbert, D. Marx and M. Havenith, *J. Chem. Phys.*, 2013, **139**, 154304.
8 J. Elm, J. Kubečka, V. Besel, M. J. Jääskeläinen, R. Halonen, T. Kurten and H. Vehkamäki, *J. Aerosol Sci.*, 2020, **149**, 105621.
9 E. G. Schnitzler and W. Jäger, *Phys. Chem. Chem. Phys.*, 2014, **16**, 2305–2314.
10 A. K. Huff, N. Love and K. R. Leopold, *J. Phys. Chem. A*, 2021, **125**, 8033–8046.
11 C.-I. Huang, J.-Y. Feng, Y.-P. Lee and T. Ebata, *J. Phys. Chem. A*, 2023, **127**, 9550–9563.
12 L. George and W. Sander, *Spectrochim. Acta A*, 2004, **60**, 3225–3232.
13 Ł. Szyc, M. Yang, E. T. J. Nibbering and T. Elsaesser, *Angew. Chem., Int. Ed.*, 2010, **49**, 3598–3610.
14 T. L. Fischer, M. Bödecker, S. M. Schweer, J. Dupont, V. Lepère, A. Zehnacker-Rentien, M. A. Suhm, B. Schröder, T. Henkes, D. M. Andrada, R. M. Balabin, H. K. Singh, H. P. Bhattacharyya, M. Sarma, S. Käser, K. Töpfer, L. I. Vazquez-Salazar, E. D. Boittier, M. Meuwly, G. Mandelli, C. Lanzi, R. Conte, M. Ceotto, F. Dietrich, V. Cisternas, R. Gnanasekaran, M. Hippler, M. Jarraya, M. Hochlaf, N. Viswanathan, T. Nevolianis, G. Rath, W. A. Kopp, K. Leonhard and R. A. Mata, *Phys. Chem. Chem. Phys.*, 2023, **25**, 22089–22102.
15 L. Evangelisti, L. Spada, W. Li, F. Vazart, V. Barone and W. Caminati, *Angew. Chem., Int. Ed.*, 2017, **56**, 3872–3875.
16 S. M. Schweer, M. Gawrilow, A. Nejad and M. A. Suhm, *Phys. Chem. Chem. Phys.*, 2023, **25**, 29982–29992.
17 K. Haupa, A. Bil, A. Barnes and Z. Mielke, *J. Phys. Chem. A*, 2015, **119**, 2522–2531.
18 K. Töpfer, S. Käser and M. Meuwly, *Phys. Chem. Chem. Phys.*, 2022, **24**, 13869–13882.
19 H. Pašalić, D. Tunega, A. J. A. Aquino, G. Haberhauer, M. H. Gerzabek and H. Lischka, *Phys. Chem. Chem. Phys.*, 2012, **14**, 4162–4170.
20 M. Katada and A. Fujii, *Chem. Phys. Lett.*, 2017, **684**, 368–372.
21 E. G. Tarakanova, G. I. Voloshenko, I. S. Kislina, V. D. Mayorov, G. V. Yukhnevich and A. K. Lyashchenko, *J. Struct. Chem.*, 2019, **60**, 225–267.
22 K. Li, J. Ďurana, B. Kocábková, A. Pysanenko, Y. Yan, M. Ončák, M. Fárník and J. Lengyel, *Chem. Phys. Chem.*, 2024, **25**, e202400071.
23 S. M. Schweer, A. Nejad and M. A. Suhm, *Phys. Chem. Chem. Phys.*, 2022, **24**, 26449–26457.
24 M. E. Wolf, J. M. Turney and H. F. Schaefer, *Phys. Chem. Chem. Phys.*, 2020, **22**, 25638–25651.
25 S. Lopes, R. Fausto and L. Khriachtchev, *J. Chem. Phys.*, 2016, **144**, 084308.
26 Z. Zhou, Y. Shi and X. Zhou, *J. Phys. Chem. A*, 2004, **108**, 813–822.
27 F. Ito, *J. Mol. Struct.*, 2016, **1118**, 161–166.
28 E. L. Sibert III, *J. Chem. Phys.*, 2019, **150**, 090901.
29 T. L. Fischer, T. Wagner, H. C. Gottschalk, A. Nejad and M. A. Suhm, *J. Phys. Chem. Lett.*, 2021, **12**, 138–144.
30 P. O. Åstrand, G. Karlström, A. Engdahl and B. Nelander, *J. Chem. Phys.*, 1995, **102**, 3534–3554.
31 N. O. Lüttschwager, *JOSS*, 2021, **6**, 3526.
32 S. Grimme, J. Antony, S. Ehrlich and H. Krieg, *J. Chem. Phys.*, 2010, **132**, 154104.
33 S. Grimme, S. Ehrlich and L. Goerigk, *J. Comput. Chem.*, 2011, **32**, 1456–1465.
34 F. Weigend and R. Ahlrichs, *Phys. Chem. Chem. Phys.*, 2005, **7**, 3297–3305.
35 F. Neese, *WIREs Comput. Mol. Sci.*, 2022, **12**, e1606.
36 M. Gawrilow and M. A. Suhm, *Phys. Chem. Chem. Phys.*, 2020, **22**, 15303–15311.
37 M. Gawrilow and M. A. Suhm, *Molecules*, 2021, **26**, 4523.
38 N. O. B. Lüttschwager, *Phys. Chem. Chem. Phys.*, 2024, **26**, 10120–10135.
39 K. E. Otto, Z. Xue, P. Zielke and M. A. Suhm, *Phys. Chem. Chem. Phys.*, 2014, **16**, 9849–9858.
40 H. C. Gottschalk, T. L. Fischer, V. Meyer, R. Hildebrandt, U. Schmitt and M. A. Suhm, *Instruments*, 2021, **5**, 12.
41 S. Oswald, E. Meyer and M. A. Suhm, *J. Phys. Chem. A*, 2018, **122**, 2933–2946.

42 K. Marushkevich, L. Khriachtchev, J. Lundell, A. Domanskaya and M. Räsänen, *J. Mol. Spectrosc.*, 2010, **259**, 105–110.
43 K. Marushkevich, L. Khriachtchev and M. Räsänen, *J. Phys. Chem. A*, 2007, **111**, 2040–2042.
44 K. A. E. Meyer and M. A. Suhm, *Chem. Sci.*, 2019, **10**, 6285–6294.
45 W. H. Robertson, J. A. Kelley and M. A. Johnson, *J. Chem. Phys.*, 2000, **113**, 7879–7884.
46 M. Bödecker, D. Mihrin, M. A. Suhm and R. Wugt Larsen, *J. Phys. Chem. A*, 2024, **128**, 7124–7136.
47 D. W. Michael and J. M. Lisy, *J. Chem. Phys.*, 1986, **85**, 2528–2537.
48 T. Häber, U. Schmitt, C. Emmeluth and M. A. Suhm, *Faraday Disc.*, 2001, **118**, 331–359.
49 J. Krupa, I. Kosendiak, M. Wierzejewska and J. Lundell, *Spectrochim. Acta A*, 2025, **325**, 125081.
50 A. Nejad, E. Meyer and M. A. Suhm, *J. Phys. Chem. Lett.*, 2020, **11**, 5228–5233.
51 E. Sánchez-García, M. Studentkowski, L. A. Montero and W. Sander, *Chem. Phys. Chem.*, 2005, **6**, 618–624.
52 C. V. Berney, R. L. Redington and K. C. Lin, *J. Chem. Phys.*, 1970, **53**, 1713–1721.
53 S. Trabelsi, M. Tlili, F. Hammami, S. Nasr, M.-C. Bellissent-Funel and J. Darpentigny, *J. Chem. Phys.*, 2023, **159**, 224503.
54 D. K. Maity, *J. Phys. Chem. A*, 2013, **117**, 8660–8670.
55 A. Patla, D. Kumari, A. Kumar, R. Jana and R. Subramanian, *Mol. Phys.*, 2025, **0**, e2478202.
56 B. X. Shi, F. Della Pia, Y. S. Al-Hamdani, A. Michaelides, D. Alfè and A. Zen, *J. Chem. Phys.*, 2025, **162**, 144107.